Temporal dynamics of mRNA translation dysregulation and codon decoding during murine stroke evolution.

Sherif Rashad[1,2]#*, Yuki Kitamura[1-3]*, Tomohito Nagai[1-3], Daisuke Ando[1,2,4,5], Abdulrahman Mousa[1], Hajime Ikenouchi[1,4], Hidenori Endo[3], Kuniyasu Niizuma[1-3,5]

1- Department of Neurosurgical Engineering and Translational Neuroscience, Tohoku University Graduate School of Medicine, Sendai, Japan.
2- Department of Neurosurgical Engineering and Translational Neuroscience, Graduate School of Biomedical Engineering, Tohoku University, Sendai, Japan.
3- Department of Neurosurgery, Tohoku University Graduate School of Medicine, Sendai, Japan.
4- Department of Neurology, Tohoku University Graduate School of Medicine, Sendai, Japan
5- Division of Development and Discovery of Interventional Therapy, Tohoku University Hospital

*** Equal contribution**

#Corresponding author:

Sherif Rashad, MD, PhD

Sherif.mohamed.rashad.e3@tohoku.ac.jp

Abstract

Ischemic stroke is the second leading cause of mortality worldwide, yet there are limited neuroprotective therapeutics available. Ischemic stroke triggers rapid and complex molecular changes, yet the dynamics of mRNA translation during stroke remain largely unexplored. Here, we present the first temporal ribosome profiling (Ribo-seq) analysis in a murine distal middle cerebral artery occlusion (dMCAO) model, assessing translational regulation at 1-, 6-, and 24-hours post-stroke. We identified distinct stage-specific phenomena, including a hyperacute GC-ending codon bias and a transient burst of stop-codon readthrough (SCRT) at 1-hour, predominantly affecting neuronal and synaptic pathways, and an activation of pathways linked to vascular remodeling and endothelial function. From 6-hours onward, we observed progressive ribosome pausing, altered elongation dynamics, and widespread frameshifting affecting mitochondrial, synaptic, and metabolic genes, coinciding with strong immune pathway activation. These events cannot be evaluated at the level of transcript abundance, underscoring the value of translation-focused approaches. Our findings reveal that translational control in stroke follows a phased program, with multiple regulatory and maladaptive phenomena impacting the gene expression and outcome of stroke. This work uncovers hidden layers of translational regulation in stroke pathophysiology and identifies potential mechanistic targets that could be explored for potential therapeutics development.

Keywords:

Stroke; Stop codon readthrough; Codon bias; Neurons; Frameshifting; Ribosome; Ribo-seq.

Introduction

Ischemic stroke (IS) is one of the leading causes of morbidity and mortality worldwide[1]. Treatment strategies for IS have evolved rapidly in the past two decades and led to great improvements in the outcomes of stroke patients[2,3]. Nonetheless, there is a global upward trend in IS especially in low to middle income countries[4]. IS pathophysiology is multifaceted and complex and includes a cascade of responses in neurons, microglia, astrocytes, and other brain cells[5]. A hallmark of IS is the activation of programmable cell death in neurons due to extensive excitotoxicity and oxidative stress, as well as neuroinflammation driven by microglia[5,6]. In addition to the need for regenerative therapies for stroke[7], there is a pressing need to develop novel neuroprotective therapies that can protect neurons and reverse the damage induced by brain ischemia[5,8]. To date, neuroprotective therapies have not been widely available, which could be attributed to our incomplete understanding of stroke pathophysiology and its complex evolving nature. Despite a wealth of studies utilizing RNA sequencing and single cell RNA sequencing methods[9-11] that has greatly enhanced our understanding of stroke pathophysiology, efforts to reveal the translational patterns of mRNA during stroke are virtually absent from the literature. Recently, it became understandable that during acute stress, there is a disconnect between mRNA levels and actual mRNA translation[12]. Thus, technologies focusing on mRNA translation, such as Ribo-seq, provide a much better insights to the cellular phenotype and the cellular proteome than gene expression centric methods[13,14].

During oxidative stress, various epitranscriptional and post-transcriptional machinery are activated to regulate gene expression and drive the translation of antioxidant defense systems[12,15]. For example, the tRNA epitranscriptome has been a subject of great interest, given its influence on regulating codon decoding and driving mRNA translation during stress independently from gene expression levels[12,15-19]. Previously, we have shown that during ischemic stroke, tRNA is cleaved to generate tRNA derived small non-coding RNAs (tDRs)[20,21]. Such findings allude to potential translation and epitranscriptional processes being at play in stroke pathophysiology. However, to date, no studies have attempted to evaluate the translatome or the epitranscriptome in depth in the context of IS, leaving a large gap in our understanding of stroke pathology.

In this work, we evaluated the temporal mRNA translational dynamics in mouse model of IS. We conducted Ribo-seq analysis, which, to our surprise, was not done previously in the context of stroke, to elucidate various translational changes occurring during stroke. Our work uncovered various translational deregulatory phenomena that occur during IS. Understanding these phenomena, and their regulation, would prove vital in understanding the pathophysiology of Stroke and in developing novel therapeutics.

Results

- **Temporal dynamics of translation reflects hyperacute translation dysregulation and acute immune response**

To study the translational dynamics of stroke evolution, we utilized the distal middle cerebral artery occlusion model (dMCAO) and collected brain samples for analysis after 1, 6, and 24 hours of stroke induction [Figure 1A]. We observed brain infarct 24 hours after dMCAO induction using TTC stain [Figure 1B]. We conducted Ribo-seq using sham treated animals as well as 1, 6, and 24 hours after dMCAO induction (N = 4 per group. Annotation in figures: 1 hour = H1, 6 hours = H6, 24 hours = H24). Metagene plots showed clear 3-nucleotide periodicity in all samples/groups [Figure 1C], validating the detection of ribosome protected fragments in our sequencing and its quality. To elucidate the differentially translated genes (DTGs) after dMCAO, we counted only the protein coding sequences, using the tag "-t CDS" with featureCounts[22]. Heatmap clustering using DESeq2[23] normalized gene counts showed clustering of sham and 1 hour groups together, while the later time points (6 and 24 hours) clustered together [Figure 1D]. DTG analysis revealed progressive changes in mRNA translation profiles as Stroke progressed, with more mRNAs being translated in later time points [Figure 1E-G, Supplementary figure 1]. It was also evident that there was minimal overlap between the DTGs at 1 hour and at 6 and 24 hours [Supplementary figure 1]. Spearman's correlation validated these findings, where the correlation between 1 hour and 6 or 24 hours was modest ($\rho = 0.447$ and 0.428 respectively) while it was strongest between 6 and 24 hours ($\rho = 0.78$) [Supplementary figure 1B-D].

We next conducted overrepresentation analysis (ORA analysis) on the upregulated genes at each time point (Threshold for significance: FDR < 0.05, "Log2 fold change| > 1) [Supplementary figure 2]. 1-hour after stroke, we observed the upregulation of pathways linked to endothelial and smooth muscle proliferation and migration. These could be linked to blood brain barrier (BBB) breakdown that occurs in stroke. We did not, on the other hand, observe activation of stress pathways in the neurons or any changes in neuronal-specific pathways. From 6 hours onwards, we observed a very strong immune signature with pathways linked to leukocyte migration and activation being significantly upregulated. Only at the 24 hours mark we observed

downregulation of pathways linked to synaptic functions, signifying neuronal cell death and dysfunction [Supplementary figure 2D].

In summary, our DTG analysis reveals progressive activation of the immune response after stroke with no clear activation of stress response pathways in the neurons.

- **Alterations in codon decoding after stroke**

To elucidate the impact of stroke on translation at the level of codon decoding, we employed several metrics to assess codon decoding, bias, and optimality. First, we evaluated A-site pausing or ribosome dwelling times at the A-site, which can give important clues on decoding speed and translation. At the 1-hour mark, we did not observe significant ribosome pausing. However, at the later time points, we observed progressive ribosome pausing, especially at hydrophobic amino acids codons like Leucine and Alanine codons [Figure 2A-C]. Next, we evaluated AT-ending vs GC-ending codon bias. During stress, there is a translational bias towards GC-ending codon to activate various stress pathways[12,16]. While our ORA analysis did not show clear signs of stress pathways upregulation, we observed GC-ending codon biased translation 1 hour after stroke using GC3 score analysis [Figure 2D]. GC3 score is a simple score counting the number of GC-ending codons in each mRNA sequence, going from 0 (all codons are AT-ending) to 1 (all codons are GC-ending). This pattern of GC-biased translation was not observed in later time points after stroke. Another metric, isoacceptors frequencies analysis, validated these findings. Isoacceptors frequencies are calculated by comparing synonymous codons representation in mRNA sequences. After subsetting for significant genes, we compared the isoacceptors frequencies for those genes to the whole genome (background) to identify statistically significant enriched codons in the up or downregulated genes. In our analysis, we observed global AT-ending vs GC-ending codon bias [Figure 2G]. However, only at 1 hour we observed opposing patterns between the up and downregulated genes, while at 6 or 24 hours, the codon patterns between the up and downregulated genes were essentially the same.

In summary, our analysis reveals progressive ribosome pausing, indicative of translational dysregulation, as stroke progresses. Our analysis also shows characteristic codon bias towards GC-ending codons, which could be linked to the activation of endothelial differentiation pathways[24].

- **Stroke impacts translation elongation**

Analysis of Ribo-seq reads themselves does not give a full picture of the changes in translation dynamics. Particularly, the rate of elongation of ribosomes across the CDS is a critical information to understand the influence of mRNA translation on the proteome, since elongation rates are coupled to efficient translation. First, we examined the ribosome occupancy downstream from the start codon and upstream from the stop codon. We observed that after stroke, there is a significant increase in ribosome occupancy downstream from the start codon compared to sham animals. On the contrary, the occupancy decreased towards the stop codon [Figure 3A]. This suggests that stroke may cause translation elongation defects.

Typically, elongation rates are analyzed using pulse-chase experiments *in vitro*[25], however, such approaches are not suitable for complex multicellular organisms. To identify genes that show significant differences in their elongation rates, we divided the CDS into 3 bins and calculated the counts for each gene in each biological sample across the 3 bins. Then, we generated the elongation ratio (ER) using the formula shown in Figure 3B (see methods). ER > 1 indicates that most of the RPF counts of the gene are in the second two thirds of the CDS. ER < 1 indicates that most of the RPF counts are towards the first third of the CDS. Thus, we reasoned that genes with higher ER have better elongation dynamics. Importantly, the ER score is internal to each gene, and thus global changes in gene RPF counts between samples, which are used for DTG analysis, do not have an impact on it. We used Mann-Whitney U test to compare between each time point and the sham. In that analysis, upregulated genes would have better elongation dynamics (i.e. most RPF reads are in the later 2/3 of the CDS) compared to sham and vice versa. We observed progressive alterations in the elongation scores of hundreds of genes, signifying potential changes in elongation dynamics, after stroke, reaching the maximum after 24 hours (significance indicated by $|\text{Log2FC}| \geq 1$ and $p < 0.05$) [Figure 3C]. ORA analysis revealed that at 1 hour, there was downregulation of transport related pathways and metabolic pathways 1 hour after stroke [Supplementary figure 3A]. This was followed by downregulation of processes related to nucleotide and ATP biosynthesis and energy metabolism at 6 hours [Supplementary figure 3B]. On the other hand, pathways related to synaptic transport and activity, and cellular respiration were upregulated after 6 hours [Supplementary figure 3C]. 24 hours after stroke, we observed

downregulation of pathways related to synaptic activity and transport [Figure 3D] and upregulation of pathways related to response to stress and metal ions (which could indicate ferroptosis cell death[26]) and regulation of various processes related to protein function.

We further explored whether the changes in elongation dynamics are linked to codon usage and optimality. We conducted isoacceptors frequencies analysis on the significant genes in our dataset. We did not observe significant differences in the codon usage between the up and downregulated genes [Figure 3F]. While there were some observed biases 1 hour after stroke, it was not statistically significant (T-statistic not > 2 or < -2).

In summary, we observed changes in elongation dynamics not linked to codon usage or bias after stroke. The pathways impacted differ from those observed at the DTG level, indicating the various mechanisms by which stroke molecular pathophysiology impacts translation.

- **Stroke leads to transcriptome-wide reading frame alterations**

Alterations in the reading frame can introduce premature termination codons (PTCs) and activation of none-sense mediated decay (NMD) or lead to the generation of alternative proteoforms with new functions or loss of function[27-29]. We argued that the severe metabolic stress induced by stroke induction could alter the reading frames in the brain, with varying downstream effects. To identify whether stroke induces frameshifting in the reading frame of specific genes or gene sets, we designed a python script that calculates the P-site offset by adapting the method employed by RiboWaltz[30], then counted for each gene the number RPFs mapping to each frame (0, +1, or +2). We then calculated the frameshift score (FS, see methods section), so that genes with higher FS have more reads in the +1 and/or +2 frames compared to the 0 frame (i.e. frameshifted). We filtered to include only genes having ≥ 20 reads in at least 3 of the 4 biological replicates in a group, then we used the final 9813 genes to conduct Mann-Whitney U test to compare each condition with the sham group. Upregulated genes indicate genes that have more reads in the +1 or +2 frames compared to sham and downregulated genes indicate genes that have more reads in the 0 frame compared to sham.

We observed minimal changes in the reading frame 1 hour after stroke. However, from 6 hours onwards, we observed massive changes in the reading frame impacting 21~26% of the

detected genes passing our filter [Figure 4A-D]. Codon analysis did not yield a specific pattern either in GC3 analysis [Figure 4E] or isoacceptors analysis [Supplementary figure 4A] that could be linked to alterations in the reading frame. We examined the pathways impacted by the observed frameshifting using ORA analysis. 6 hours after stroke we observed downregulation of pathways linked to synapses and vesicle transport and other neuronal pathways, while there was a significant frameshifting in pathways linked to energy metabolism, synaptic structure, and mitochondrial function [Figure 4F-G]. 24 hours after stroke we observed downregulation of pathways linked to translation with upregulation of pathways linked to energy metabolism, mitochondrial and synaptic structure [Figure 4H-I].

In summary, we observed changes in the reading frames of a large percentage of detected genes in the acute stage after stroke. These changes can be linked to known pathophysiological mechanisms such as mitochondrial dysfunction, neuronal dysfunction, and energy stress that occur after stroke. However, the cause of these changes is not due to codon sequences. Nonetheless, the full impact of these aberrations is yet to be understood.

- **Stroke leads to stop codon readthrough (SCRT)**

Dysregulated translational dynamics and reading frames could lead to stop codon readthrough (SCRT), where the ribosomes fail to end translation at the stop codon and continue translating into the 3'UTR region until it faces another termination codon downstream[31]. We analyzed SCRT events after stroke by counting the reads that map to the 3'UTR and comparing them to the reads that map to the CDS for each gene [Figure 5A]. We applied a stricter filtering step, selecting genes with ≥ 100 reads to be included in the analysis, yielding a matrix with 7943 genes. We then used Mann-Whitney U test to compare between each condition and the sham group. Upregulation indicates more SCRT events per gene compared to sham and downregulation is the opposite. We observed significant upregulation of SCRT events 1 hour after stroke, with fewer numbers of SCRT events in later timepoints [Figure 5B]. While we observed significant numbers of downregulated genes in our SCRT analysis at 6 and 24-hour timepoints, it could be an artifact. Thus, to evaluate whether SCRT are real or an analytic artifact, we generated metagene profiles extending into the 3'UTR to observe the presence of real P-sites, indicating translating ribosomes. We observed true ribosome footprints downstream of the stop codons only in the 1-hour group

[Figure 5C]. These footprints extended well beyond the stop codon and were observed up to 100 nucleotides in the 3'UTR, indicating that they are true SCRT and not simple ribosome stalls at the stop codons due to failure of release. We also investigated few hit genes to observe the P-sites in the 3'UTR. For example, in Ercc6, shown in Figure 5D, and Mrpl10, shown in Figure 5E, we can clearly observe RPFs in the 3'UTRs indicating SCRT that are > 50~100 nucleotides downstream of the stop codon. To examine what pathways could be linked to the SCRT observed after 1 hour of stroke, we conducted ORA analysis, which revealed alterations in pathways linked to synaptic function, vesicle and protein transport, and cytoskeletal organization, all linked to neuronal function. Thus, given the potential impact of the addition of extra amino acids to the protein sequence on structure and function, SCRT could deregulate neuronal function before clear downregulation of neuronal pathways is observed.

To identify why SCRT events happen, we first examined the gene hits using GC3 analysis, which did not reveal any clear alteration with mean GC3 scores of the significant genes with SCRT around 0.5~0.6 (i.e. the genome average) [Figure 6B]. Isoacceptors codon frequencies analysis revealed that certain codons were significantly enriched in the upregulated genes compared to the genome average (i.e., with more SCRT events) [Figure 6C]. The top codons linked to SCRT were Arg-CGA and Leu-TTA.

To understand the root causes of SCRT changes, we examined the stop codon context of the significant genes at each time point. Here, we examined the sequence of the stop codon, as well as the 5 codons upstream and 5 codons downstream of the stop codon. We then conducted fisher's test to compare between the upregulated genes 1 hour after stroke and the background (all genes). Our analysis revealed several codons that are present upstream and downstream from the stop codon at significantly higher percentages compared to the genome average [Figure 6D]. How the presence of these codons impact SCRT remains to be seen.

In summary, we observed significant SCRT events occurring in the hyperacute stage after stroke, mainly impacting neuronal functions, before other translational clues that the neuronal function is impacted significantly. The SCRT appear to be linked to specific codon sequences, however, such assumptions need to be further examined.

Discussion

Despite wealth of literature on ischemic stroke (IS) pathophysiology, mRNA translational changes during stroke remain an understudied area. In fact, to date, there have not been studies that utilized Ribo-seq to study animal models of stroke. Thus, our understanding of stroke pathophysiology remains incomplete. Here, in this work, we provide the first analysis of IS in a murine model using Ribosome protected fragments (RPF) sequencing (or Ribo-seq as referred to herein). In our analysis, we explored not only the changes in the rates of translation, i.e. differential translation of genes (DTGs), but expanded our analysis to various phenomena occurring at the level of mRNA translation that could explain the dysregulated proteome and neuronal dysfunction in consequence to IS. Our analysis revealed a strong immune signature that is activated after stroke. Nonetheless, there have been several notable attempts to understand the translational changes that occur during stroke. Two studies have used Ribo-Tag mice to isolate translating ribosomes from endothelial cells[32] and from astrocytes[33] after mouse models of stroke. However, both studies, while offering important cell-specific information on stroke pathogenesis, relied on ribosome pull down and simple RNA sequencing of translated mRNAs. Thus, information on ribosome decoding dynamics and other translational phenomena is not clarified. Both studies also analyzed only one time point after stroke, thus they offered no analysis of the evolution of translational changes as stroke pathology progressed from the hyperacute stress response to the acute neuronal cell death and immune activation. Thus, our analysis is the first, to the best of our knowledge, temporal analysis of translational aberrations and changes occurring in murine stroke models.

In our analysis, the changes occurring during stroke are drastic and sharp. One hour after stroke, we observed a strong codon biased translational program, with shift towards translation of G/C-ending codons, akin to what is observed in cellular models of acute oxidative stress[12,16]. However, pathway analysis revealed that this shift is probably due to a shift towards vascular proliferation pathways[24]. Indeed, acute stress response could be contributing to this codon-biased translational program, however, as our Ribo-seq is done in bulk, the pathway analysis would be skewed towards the most upregulated and dominant signatures. Perhaps the most unexpected result was the burst of stop-codon readthrough (SCRT) observed at the 1 h mark. Readthrough—producing C-terminally extended proteoforms—has been documented in viral infection, hypoxia,

and oxidative stress, mainly in prokaryotes and yeast, but has not been systematically studied in multicellular organisms or in the context acute brain injury[31,34,35]. The over-representation of Arg-CGA and Leu-TTA codons around termination sites of SCRT-prone transcripts hints that local codon context may predispose to readthrough, consistent with codon-dependent termination kinetics described in other systems[31]. While we observed SCRT events occurring in later time points, careful examination of a cohort of genes revealed no real P-sites in the 3'UTR, indicating that the effect is due to changes in translation rates (i.e. computational noise from the counting algorithm) rather than true SCRT events as those occurring at the 1-hour mark. Further analysis of the pathways impacted by SCRT revealed near exclusive enrichment of neuronal pathways, especially those linked to synaptic functions. Thus, we hypothesize that SCRT is a maladaptive event due to energy failure in the neurons in consequence to extreme oxidative stress. This observation is also a clear indication why in-depth analysis of translational changes could give clues to stroke pathophysiology that cannot be obtained otherwise.

In later time points (6- and 24-hours) we observed progressive immune activation at the translational level as well as progressive translation elongation changes, where mRNAs linked to synaptic and neuronal functions had progressively slower translational rates. Although this is done computationally, further pulse-chase Ribo-seq experiments in cellular models of stroke could further validate our *in vivo* findings[36]. We also observed significant changes in the reading frames of ribosome in the later time points. These changes mainly impacted neuronal, mitochondrial, and energy pathways. Changes in ribosomes reading frame could modulate the translation of these pathways via activating mRNA decay[37]. Further analysis using deep proteomics and other orthogonal methods could shed light on the presence or absence of truncated proteins, which could also act as immunopeptides to activate the immune system[38].

One of the main limitations of our work is the lack of cellular resolution of our analysis. While certain phenomena could be attributed to specific cell types based on the genes/pathways analysis, our assumptions need to be validated via methods such as Ribo-tag based Ribo-seq approaches or spatial RNA/Ribo-seq methods[39]. In addition, the impact of the discovered phenomena such as SCRT or frameshifting in Stroke context is not understood and should be further studied using orthogonal and focused approaches. Future work focusing on these phenomena using various cellular and animal modeling approaches, as well as complementing

our findings with spatial omics and deep proteomics will greatly enhance our understanding of Stroke pathophysiology.

In summary, our work reveals multiple hidden layers of regulation of stroke pathophysiology. Integrating these findings into our existing models of stroke molecular pathology, identifying their regulatory mechanisms, understanding their impact on the pathology, and identifying modalities to target such aberrations of translation could prove vital in developing next generation stroke therapeutics.

Methods:

Animals

Distal middle cerebral artery occlusion (dMCAO) was induced on the left side in 12-week-old, 20-25 g male C57BL/6JJmsSlc mice as previously described[40]. Animals were bought from a local vendor (Kumagai-Shoten Sendai) and housed in a controlled environment with a 12 h light/dark cycle and temperature regulated at 23 ℃. Animals were allowed to acclimatize for at least 1 week before surgery. All experiments were conducted according to protocols approved by the animal care facility of Tohoku University (Ethical approval number 2024-医工動-005-01), the Animal Research: Reporting of In Vivo Experiments guidelines, and the Code of Ethics of the World Medical Association.

dMCAO surgery

The permanent MCAO model was performed according to previous reports[40,41]. Briefly, mice were anesthetized with 2% isoflurane (30% oxygen, 70% nitrous oxide). Rectal temperature was maintained at 37℃ using a heating pad with feedback control during surgery. The temporalis muscle between the left eye and ear was retracted along a 4-mm skin incision. A small bone window (~1 mm diameter) was drilled to expose the distal MCA. The MCA was cauterized using bipolar electrocoagulation distal to the lenticulostriate branches. The incision was closed with 6-0 nylon sutures. Animals were monitored in a cage placed on a 37℃-heating plate for 1 h during anesthesia recovery. The left common carotid artery (CCA) was temporarily occluded with 6-0 nylon immediately before MCA cauterization and was released after 1 h.

Animals were euthanized at 1 h, 6 h, or 24 h after MCA cauterization. Sham-control animals underwent the same surgical procedure without MCA cauterization and CCA ligation and were euthanized after 1 h. A total of 16 mice were used (N=4 biological replicates per group: Sham, 1 h, 6 h, and 24 h after MCAO).

Ribo-seq library preparation:

Ribo-seq was conducted as previously described[42,43]. Briefly, at the designated time point, animals were sacrificed and perfused using ice-cold phosphate buffered saline (PBS) containing 100μg/ml cycloheximide, followed by extraction of the brain. Brains were extracted and

sectioned into three equal parts in the sagittal plane. The leftmost third of the brain, corresponding to Bregma -2 mm to +2 mm, where the infarct occurs, was immediately snap-frozen in liquid nitrogen. Dissection was conducted on ice and all tools were treated with RNAse inhibitor (RNAse away) prior to use. Tissues were homogenized in polysome lysis buffer (20 mM Tris-Cl pH 7.5, 150 mM NaCl, 5 mM $MgCl_2$, 1 mM dithiothreitol (Sigma, #D9779), 100 µg/ml cycloheximide, and 1% Triton X-100) and centrifuge at 13000 x g at 4°C for 15 min. Ribosome foot-printing was performed on the supernatant collected by adding 1.25 U/µl RNase I (NEB, #M0243L) to 500 µl clarified lysate and incubating samples on a rotator mixer for 45 min at room temperature. TRIzol reagent was added, and RNA was extracted using miRNeasy Mini Kit (QIAGEN, #217004). Ribosome protected fragments (RPFs) were selected by isolating RNA fragments of 27-35 nucleotides (nt) using TBE-Urea gel. rRNA depletion was conducted using NEBNext rRNA depletion kit v2 (NEB, #E7400L) followed by end-repair using T4 PNK after purification of the rRNA depleted samples using Oligo Clean & Concentrator Kits (Zymo research, #D4060). The preparation of sequencing libraries for ribosome profiling was conducted via the NEBNext Multiplex Small RNA Library Prep kit for Illumina according to the manufacturer's protocol (NEB, #E7300S). Pair-end sequencing reads of size 150 bp were produced for Ribo-seq on the Ilumina Hiseq X-ten system. Four biological replicates were prepared per group.

Ribosome profiling data analysis

Quality control for Raw Fastq was performed using FastQC. Next, adapter trimming and collapsing the pair-end reads into one was done using Seqprep. Trimmomatic[44] was used to further clean low-quality reads. Bowtie2[45] was used to align the reads to a reference of rRNA and tRNA genes (mm10) to remove contaminants. After that, reads were aligned to the genome (mm10 downloaded from UCSC), and reads counted using FeatureCounts[22] with the tag "-t CDS" to generate counts of protein coding genes only. Differential expression conducted using DEseq2 in R[23]. Ribotoolkit[46] and RiboWaltz[30] were used for metagene analysis, P-site offset determination, and ribosome dwelling time analysis as well as quality control of Ribo-seq samples.

GC3 and isoacceptors codon analysis

Isoacceptors frequency and total codon frequency were analyzed as we previously reported[42,43,47,48]. We used the protein coding transcript fasta from Gencode (mouse V37) to extract the coding sequences. We selected the longest transcript per gene as representative transcript for codon analysis. We used the R package coRdon to generate codon tables.

GC3 scores for each gene were calculated using this formula:

$$GC3 = \frac{N_{GC3}}{N_T}$$

Where N_{GC3} is the number of codons ending with G or C in the mRNA sequence and N_T is the total number of codons in the mRNA sequence. The GC3 score varies from 0 (no G/C-ending codons) to 1 (All codons are G/C-ending).

Isoacceptors codon frequencies were calculated as follows:

$$\text{frequency of codon } i \text{ in gene } j = \frac{\text{number of occurrences of codon } i \text{ in gene } j}{\sum_{i=1}^{n} \text{number of occurrences of isoacceptor}_{ij}}$$

where isoacceptors refers to the synonymous codons for the amino acid encoded by codon *i* and n refers to the number of isoacceptors for a given amino acid ($2 \leq n \leq 6$). The isoacceptors scores ranged from 0 to 1, representing the ratio of each synonymous codon in the mRNA sequence.

The t-statistic (T-stat) describing the codon frequency was calculated as:

$$\text{T-statistic for codon } i = \frac{x_i - \mu_i}{s_i/\sqrt{n}}$$

Where x_i refers to the mean frequency for codon *i* in the sample, μ_i refers to the mean frequency for codon *i* across the Mus musculus genome, s_i refers to the standard deviation of the frequency for codon *i* in the sample, and n refers to the sample size.
T-statistics value of > 2 or < -2 indicates statistical significance ($p < 0.05$) versus the background (i.e. all genes)

Stop codon readthrough (SCRT) analysis

To analyze stop codon readthrough events, we followed the logic proposed in previous publication[31]. We used a custom python script to extract the coding sequences (CDS) and 3'UTR regions from mouse annotation GTF file as a bed file. Next, we excluded the first 18 nucleotides after the start codon and the last 15 nucleotides before the stop codon, to avoid bias from the

large peaks observed at those regions. Next, we used bedtools to remove any possible overlap between the 3'UTR regions and the CDS annotation from potential overextension of short 3'UTRs. We created a custom python script that uses bedtools intersect to count reads in each sample that maps to either the CDS or 3'UTR. Next, the ribosome readthrough score (RRS) was calculated as such:

$$RRS = \frac{3'UTRcounts + 1e-6}{CDS\ counts + 1e-6}$$

The small value of 1e-6 was added to avoid potential mishandling of the script when zero values are present. The analysis was continued in R, where only genes with > 100 reads were included in the final matrix. Next, we used Mann-Whitney statistical test to compare each gene using the RRS scores. Statistical significance was defined as |log2FC| > 1 and $p < 0.05$. Genes with more SCRT events were designated as upregulated and vice versa.

3'UTR metagene plots per bam file and per gene were created using RiboWaltz[30] in *R*.

Stop codon context

To understand the potential impact of pre-termination codons on SCRT events, we used the significant genes identified from our SCRT analysis. Using Gencode transcript information, we analyzed the CDS and 3'UTR of each gene. We selected the longest transcript for each gene for analysis. The stop codon sequence and the 5 codons upstream and downstream of the stop codon were extracted for each gene. Codons were analyzed by the percentage of their occurrence in either upregulated (more SCRT) or downregulated (less SCRT) genes compared to all other codons, calculated using this formula:

$$Codon\ percentage = \frac{Codon\ count\ in\ a\ group\ in\ a\ frame}{All\ codons\ counts\ in\ the\ same\ group\ and\ the\ same\ frame} \times 100\%$$

Next, Fischer's exact test was used to identify statistically significant codon occurrences in both metrics.

Translation elongation analysis

To identify genes with elongation pausing or slowing, we divided the CDS into 3 bins and counted the reads of each gene RPF in each bin. Reads crossing between 2 bins were assigned to the bin containing > 50% of the read of the RPF. Next, we estimated the elongation ratio (ER) using this formula:

$$ER = \frac{Counts\ in\ bins\ 2\&3 + 1e-6}{Counts\ in\ bin\ 1 + 1e-6}$$

Thus, genes with higher ER have their RPF reads towards the second 2/3 of the CDS, while those with lower ER have most of their reads towards the first 1/3 of the CDS. The addition of 1e-6 was to avoid zero divisions that would lead to an error in the script. We filtered genes with fewer than 20 reads. Next, we used Mann-Whitney U test in *R* to analyze the differences between each group and the Sham group. Statistical significance was determined as p value < 0.05 and |log2FC| > 1. Upregulation indicates faster/better elongation and vice versa.

Gene level frameshifting analysis

To analyze frameshifted RPFs, we created a custom python script that first estimates the P-site offset using the same logic of RiboWaltz[30]. After P-site offset calculation per RPF length for each bam file, reads were counted and mapped to the P-site to determine their frame, based on their unique P-site offset in each bam file, whether it is 0, +1, or +2 frame. Frameshift Score (FS) for a gene was calculated as:

$$FS = \frac{Counts\ in\ frames + 1\ and + 2}{Counts\ in\ frame\ 0}$$

Thus, FS > 1 means frameshifting for a specific gene, while FS < 1 means in-frame reads for a gene.

After calculating FS scores and RPF counts for all samples, genes with total RPF < 20 in at least 3 biological replicates per group were discarded and the results merged into a single matrix. Gene with 0 RPF reads in the 0 frame and enough reads in the +1 and +2 frames to cross the filtering threshold were given an arbitrary FS score of 10. Mann-Whitney U test was used to compare between each condition and the sham group.

Data visualization and additional analysis

All statistical analysis, DTG analysis, Overrepresentation analysis (ORA), codon analysis, and visualizations were done in *R v4.5.*

Data availability: Raw Ribo-seq fastq files were deposited in sequence read archive (SRA; PRJNA1220332)

Code availability: Scripts used in this work are available through github: https://github.com/sr8510/Ribo-seq-analysis.git

Author contributions: S.R.: Conception and study design. Writing. Bioinformatics. Funding. Administration. Supervision. Y.K., T.N., D.A., A.M., and H.I: Experimentation and animal modeling. H.E.: critically reviewed the manuscript. K.N.: Critically reviewed the manuscript. Administration. Supervision.

Funding: This work was funded by the Japan society for the promotion of science (JSPS) grant number 23H02741 for S.R.

Acknowledgements: The authors report no conflicts of interest regarding this work.

References

1 Benjamin, E. J. *et al.* Heart Disease and Stroke Statistics-2019 Update: A Report From the American Heart Association. *Circulation* **139**, e56-e528, doi:10.1161/cir.0000000000000659 (2019).

2 Moritoyo, T. *et al.* A first-in-human study of the anti-inflammatory profibrinolytic TMS-007, an SMTP family triprenyl phenol. *Br J Clin Pharmacol* **89**, 1809-1819, doi:10.1111/bcp.15651 (2023).

3 Xiong, Y., Wakhloo, A. K. & Fisher, M. Advances in Acute Ischemic Stroke Therapy. *Circ Res* **130**, 1230-1251, doi:10.1161/circresaha.121.319948 (2022).

4 Fan, J. *et al.* Global Burden, Risk Factor Analysis, and Prediction Study of Ischemic Stroke, 1990-2030. *Neurology* **101**, e137-e150, doi:10.1212/wnl.0000000000207387 (2023).

5 Campbell, B. C. V. *et al.* Ischaemic stroke. *Nat Rev Dis Primers* **5**, 70, doi:10.1038/s41572-019-0118-8 (2019).

6 Sekerdag, E., Solaroglu, I. & Gursoy-Ozdemir, Y. Cell Death Mechanisms in Stroke and Novel Molecular and Cellular Treatment Options. *Curr Neuropharmacol* **16**, 1396-1415, doi:10.2174/1570159x16666180302115544 (2018).

7 Niizuma, K. *et al.* Randomized placebo-controlled trial of CL2020, an allogenic muse cell-based product, in subacute ischemic stroke. *J Cereb Blood Flow Metab* **43**, 2029-2039, doi:10.1177/0271678x231202594 (2023).

8 Faheem, H. *et al.* Neuroprotective effects of minocycline and progesterone on white matter injury after focal cerebral ischemia. *J Clin Neurosci* **64**, 206-213, doi:10.1016/j.jocn.2019.04.012 (2019).

9 Zheng, K. *et al.* Single-cell RNA-seq reveals the transcriptional landscape in ischemic stroke. *J Cereb Blood Flow Metab* **42**, 56-73, doi:10.1177/0271678x211026770 (2022).

10 Zhao, Y. *et al.* Single-Cell RNA-Seq Reveals Changes in Cell Subsets in the Cortical Microenvironment during Acute Phase of Ischemic Stroke Rats. *J Integr Neurosci* **22**, 128, doi:10.31083/j.jin2205128 (2023).

11 Guo, K. *et al.* Single-Cell RNA Sequencing With Combined Use of Bulk RNA Sequencing to Reveal Cell Heterogeneity and Molecular Changes at Acute Stage of Ischemic Stroke in Mouse Cortex Penumbra Area. *Front Cell Dev Biol* **9**, 624711, doi:10.3389/fcell.2021.624711 (2021).

12 Rashad, S. *et al.* Translational response to mitochondrial stresses is orchestrated by tRNA modifications. *bioRxiv*, 2024.2002.2014.580389, doi:10.1101/2024.02.14.580389 (2024).

13 Ingolia, N. T., Ghaemmaghami, S., Newman, J. R. & Weissman, J. S. Genome-wide analysis in vivo of translation with nucleotide resolution using ribosome profiling. *Science* **324**, 218-223, doi:10.1126/science.1168978 (2009).

14 Brar, G. A. & Weissman, J. S. Ribosome profiling reveals the what, when, where and how of protein synthesis. *Nat Rev Mol Cell Biol* **16**, 651-664, doi:10.1038/nrm4069 (2015).

15 Dedon, P. C. & Begley, T. J. Dysfunctional tRNA reprogramming and codon-biased translation in cancer. *Trends Mol Med* **28**, 964-978, doi:10.1016/j.molmed.2022.09.007 (2022).
16 Huber, S. M. *et al.* Arsenite toxicity is regulated by queuine availability and oxidation-induced reprogramming of the human tRNA epitranscriptome. *Proc Natl Acad Sci U S A* **119**, e2123529119, doi:10.1073/pnas.2123529119 (2022).
17 Chan, C. T. Y. *et al.* Reprogramming of tRNA modifications controls the oxidative stress response by codon-biased translation of proteins. *Nature Communications* **3**, 937, doi:10.1038/ncomms1938 (2012).
18 Torrent, M., Chalancon, G., de Groot, N. S., Wuster, A. & Madan Babu, M. Cells alter their tRNA abundance to selectively regulate protein synthesis during stress conditions. *Sci Signal* **11**, doi:10.1126/scisignal.aat6409 (2018).
19 Rashad, S. *et al.* The stress specific impact of ALKBH1 on tRNA cleavage and tiRNA generation. *RNA Biol* **17**, 1092-1103, doi:10.1080/15476286.2020.1779492 (2020).
20 Rashad, S., Tominaga, T. & Niizuma, K. The cell and stress-specific canonical and noncanonical tRNA cleavage. *J Cell Physiol* **236**, 3710-3724, doi:10.1002/jcp.30107 (2021).
21 Sato, K., Rashad, S., Niizuma, K. & Tominaga, T. Stress Induced tRNA Halves (tiRNAs) as Biomarkers for Stroke and Stroke Therapy; Pre-clinical Study. *Neuroscience* **434**, 44-54, doi:10.1016/j.neuroscience.2020.03.018 (2020).
22 Liao, Y., Smyth, G. K. & Shi, W. featureCounts: an efficient general purpose program for assigning sequence reads to genomic features. *Bioinformatics* **30**, 923-930, doi:10.1093/bioinformatics/btt656 (2014).
23 Love, M. I., Huber, W. & Anders, S. Moderated estimation of fold change and dispersion for RNA-seq data with DESeq2. *Genome Biol* **15**, 550, doi:10.1186/s13059-014-0550-8 (2014).
24 Gingold, H. *et al.* A dual program for translation regulation in cellular proliferation and differentiation. *Cell* **158**, 1281-1292, doi:10.1016/j.cell.2014.08.011 (2014).
25 Ingolia, N. T., Lareau, L. F. & Weissman, J. S. Ribosome profiling of mouse embryonic stem cells reveals the complexity and dynamics of mammalian proteomes. *Cell* **147**, 789-802, doi:10.1016/j.cell.2011.10.002 (2011).
26 Alim, I. *et al.* Selenium Drives a Transcriptional Adaptive Program to Block Ferroptosis and Treat Stroke. *Cell* **177**, 1262-1279 e1225, doi:10.1016/j.cell.2019.03.032 (2019).
27 Ren, G. *et al.* Ribosomal frameshifting at normal codon repeats recodes functional chimeric proteins in human. *Nucleic Acids Res* **52**, 2463-2479, doi:10.1093/nar/gkae035 (2024).
28 Demo, G. *et al.* Structural basis for +1 ribosomal frameshifting during EF-G-catalyzed translocation. *Nat Commun* **12**, 4644, doi:10.1038/s41467-021-24911-1 (2021).
29 Kishor, A., Fritz, S. E. & Hogg, J. R. Nonsense-mediated mRNA decay: The challenge of telling right from wrong in a complex transcriptome. *Wiley Interdiscip Rev RNA* **10**, e1548, doi:10.1002/wrna.1548 (2019).

30 Lauria, F. *et al.* riboWaltz: Optimization of ribosome P-site positioning in ribosome profiling data. *PLoS Comput Biol* **14**, e1006169, doi:10.1371/journal.pcbi.1006169 (2018).
31 Wangen, J. R. & Green, R. Stop codon context influences genome-wide stimulation of termination codon readthrough by aminoglycosides. *Elife* **9**, doi:10.7554/eLife.52611 (2020).
32 Arbaizar-Rovirosa, M. *et al.* Transcriptomics and translatomics identify a robust inflammatory gene signature in brain endothelial cells after ischemic stroke. *J Neuroinflammation* **20**, 207, doi:10.1186/s12974-023-02888-6 (2023).
33 Shim, B. *et al.* RiboTag RNA Sequencing Identifies Local Translation of HSP70 in Astrocyte Endfeet After Cerebral Ischemia. *Int J Mol Sci* **26**, doi:10.3390/ijms26010309 (2025).
34 Mangkalaphiban, K. *et al.* Transcriptome-wide investigation of stop codon readthrough in Saccharomyces cerevisiae. *PLoS Genet* **17**, e1009538, doi:10.1371/journal.pgen.1009538 (2021).
35 Zhang, H. *et al.* Metabolic stress promotes stop-codon readthrough and phenotypic heterogeneity. *Proc Natl Acad Sci U S A* **117**, 22167-22172, doi:10.1073/pnas.2013543117 (2020).
36 Ingolia, N. T., Brar, G. A., Rouskin, S., McGeachy, A. M. & Weissman, J. S. The ribosome profiling strategy for monitoring translation in vivo by deep sequencing of ribosome-protected mRNA fragments. *Nat Protoc* **7**, 1534-1550, doi:10.1038/nprot.2012.086 (2012).
37 Zhang, Y. *et al.* Ribosomes modulate transcriptome abundance via generalized frameshift and out-of-frame mRNA decay. *Mol Cell* **85**, 2017-2031.e2017, doi:10.1016/j.molcel.2025.04.022 (2025).
38 Weller, C. *et al.* Translation dysregulation in cancer as a source for targetable antigens. *Cancer Cell* **43**, 823-840.e818, doi:10.1016/j.ccell.2025.03.003 (2025).
39 Ren, J., Luo, S., Shi, H. & Wang, X. Spatial omics advances for in situ RNA biology. *Mol Cell* **84**, 3737-3757, doi:10.1016/j.molcel.2024.08.002 (2024).
40 Kato, Y. *et al.* Intravenous administration of muse cells improves cerebral ischemia outcome via immunomodulation in the spleen. *J Cereb Blood Flow Metab*, 271678x241290363, doi:10.1177/0271678x241290363 (2024).
41 Taguchi, A. *et al.* A Reproducible and Simple Model of Permanent Cerebral Ischemia in CB-17 and SCID Mice. *J Exp Stroke Transl Med* **3**, 28-33, doi:10.6030/1939-067x-3.1.28 (2010).
42 Ando, D. *et al.* Decoding Codon Bias: The Role of tRNA Modifications in Tissue-Specific Translation. *Int. J. Mol. Sci.* **26**, 706 (2025).
43 Zhou, Y. *et al.* Dynamic mRNA Stability Buffer Transcriptional Activation During Neuronal Differentiation and Is Regulated by SAMD4A. *J Cell Physiol*, doi:10.1002/jcp.31477 (2024).
44 Bolger, A. M., Lohse, M. & Usadel, B. Trimmomatic: a flexible trimmer for Illumina sequence data. *Bioinformatics* **30**, 2114-2120, doi:10.1093/bioinformatics/btu170 (2014).

45 Langmead, B. & Salzberg, S. L. Fast gapped-read alignment with Bowtie 2. *Nat Methods* **9**, 357-359, doi:10.1038/nmeth.1923 (2012).

46 Liu, Q., Shvarts, T., Sliz, P. & Gregory, R. I. RiboToolkit: an integrated platform for analysis and annotation of ribosome profiling data to decode mRNA translation at codon resolution. *Nucleic Acids Res* **48**, W218-W229, doi:10.1093/nar/gkaa395 (2020).

47 Rashad, S. *et al.* Codon Usage and mRNA Stability are Translational Determinants of Cellular Response to Canonical Ferroptosis Inducers. *Neuroscience* **501**, 103-130, doi:10.1016/j.neuroscience.2022.08.009 (2022).

48 Tumu, S., Patil, A., Towns, W., Dyavaiah, M. & Begley, T. J. The gene-specific codon counting database: a genome-based catalog of one-, two-, three-, four- and five-codon combinations present in Saccharomyces cerevisiae genes. *Database* **2012**, doi:10.1093/database/bas002 (2012).

Figure legends:

Figure 1: A: Schematic showing the method for generating the stroke model and the time points for collection of samples for Ribo-seq analysis. **B:** 2,3,5-Triphenyltetrazolium chloride (TTC) staining of freshly extracted and dissected brains showing the region of ischemia (in white) in the cerebral cortex 24 hours after model induction. **C:** P-site metagene plots for each of the time points studied showing the 3-nucleotide periodicity classical of Ribo-seq data (Each metagene is a summary of 4 biological replicates per group). **D:** Heatmap of the normalized read counts of each group showing the clustering of the 1-hour (H1) and sham time points versus the 6- (H6) and 24-hour (H24) groups. The color bar represents row z-score. **E-G:** Volcano plots of differentially translated genes (DTGs) in each time point versus the sham group. Significance was defined as $|\log2FC| \geq 1$ and $FDR \leq 0.05$.

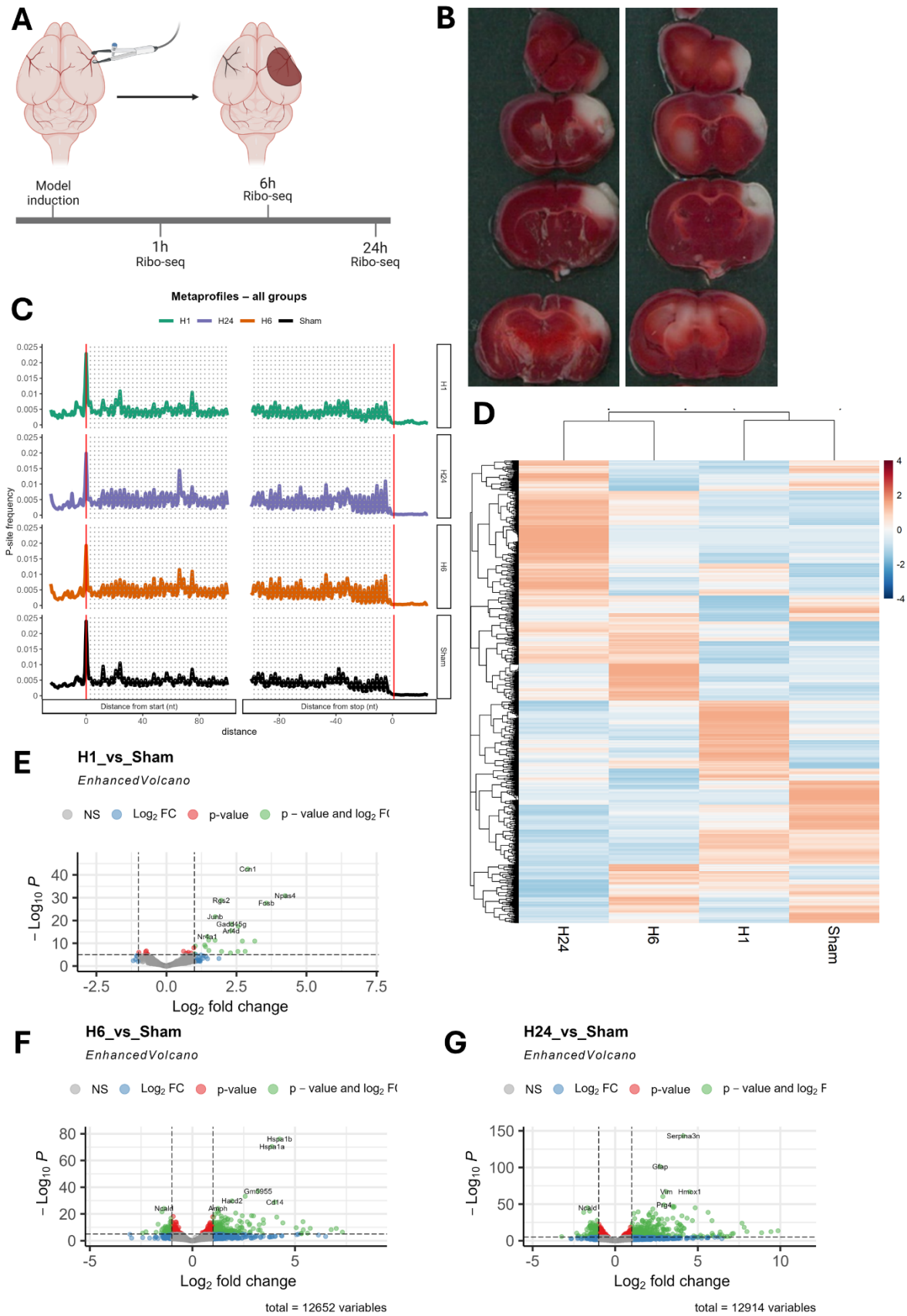
A
Model induction
6h Ribo-seq
1h Ribo-seq
24h Ribo-seq
B
C
Metaprofiles – all groups
H1
H24
H6
Sham
P-site frequency
Distance from start (nt)
Distance from stop (nt)
distance
D
H24
H6
H1
Sham
E
H1_vs_Sham
EnhancedVolcano
NS
Log2 FC
p-value
p – value and log2 FC
– Log10 P
Log2 fold change
F
H6_vs_Sham
EnhancedVolcano
NS
Log2 FC
p-value
p – value and log2 FC
– Log10 P
Log2 fold change
total = 12652 variables
G
H24_vs_Sham
EnhancedVolcano
NS
Log2 FC
p-value
p – value and log2 FC
– Log10 P
Log2 fold change
total = 12914 variables

Figure 2: Analysis of codon translation dynamics after stroke. A-C: A-site pausing compared to sham after stroke. The red highlighted codons are those of hydrophobic amino acids. **D-F:** GC-3 analysis of significantly up and downregulated genes after stroke at each time point. **G:** Isoacceptors codon frequencies analysis of the significantly up and downregulated genes after stroke at each time point. The color bar represents T-statistic compared to the genome. |T-statistic| ≥ 2 indicates statistical significance ($p \leq 0.05$).

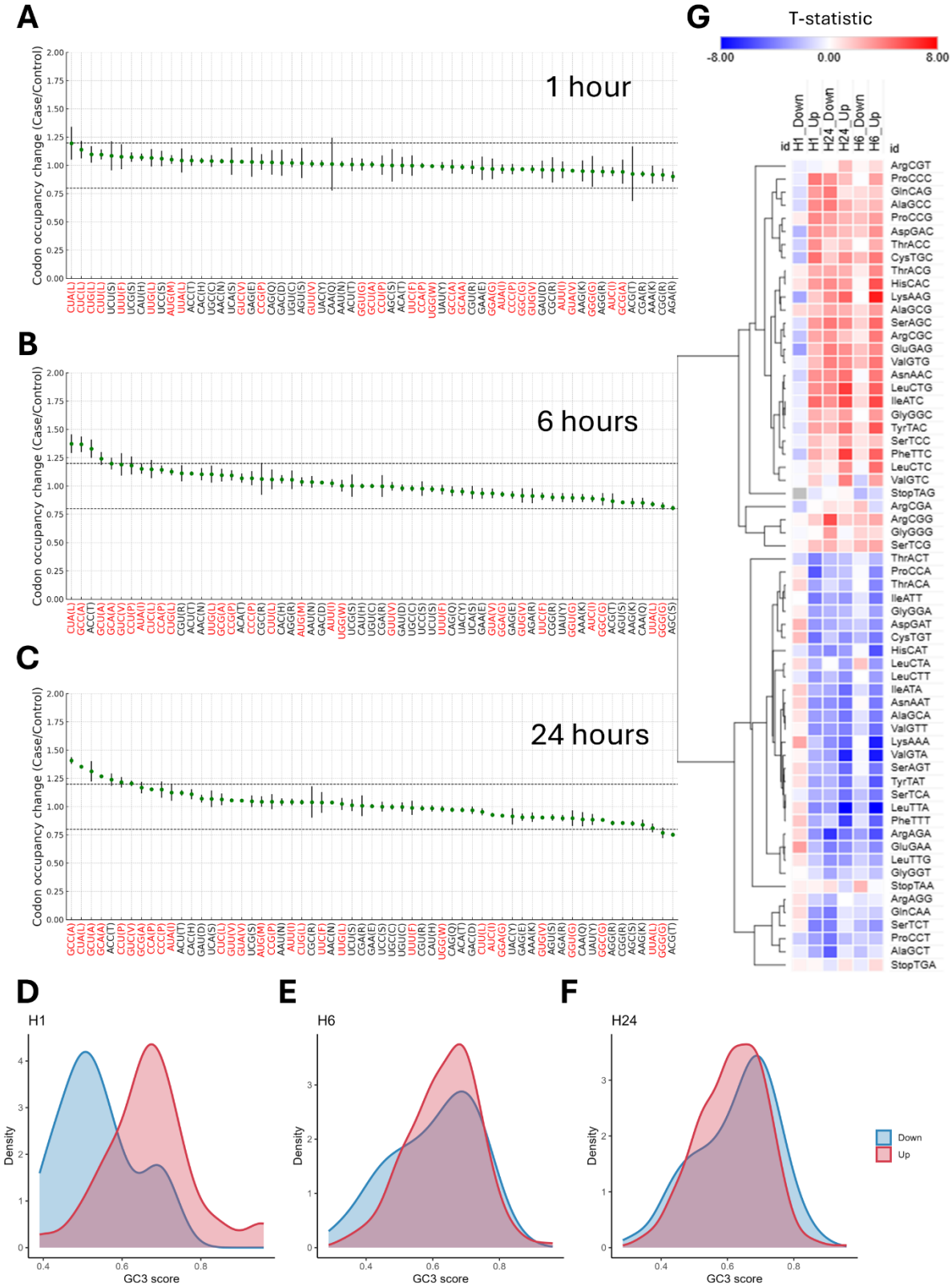
A
1 hour
B
6 hours
C
24 hours
Codon occupancy change (Case/Control)
G
T-statistic
-8.00
0.00
8.00
id
H1_Down
H1_Up
H24_Down
H24_Up
H6_Down
H6_Up
D
H1
E
H6
F
H24
Density
GC3 score
Down
Up

Figure 3: A: Ribosome occupancy metagene plots downstream of the start codon (Start) and upstream of the stop codon (End) of the CDS showing changes at each time point compared to sham. **B:** schematic of the method for analyzing elongation ratio and calculation of the gene-level elongation dynamics. **C:** Table showing the number of genes with significant changes in elongation rates. Upregulated genes indicate genes with faster/better elongation, while downregulated genes are the opposite. **D-E:** ORA-GOBP analysis of genes with statistically significant changes in their elongation dynamics in the 24-hour group versus Sham. **F:** Isoacceptors codon frequencies analysis of up or down regulated genes in the elongation rate analysis.

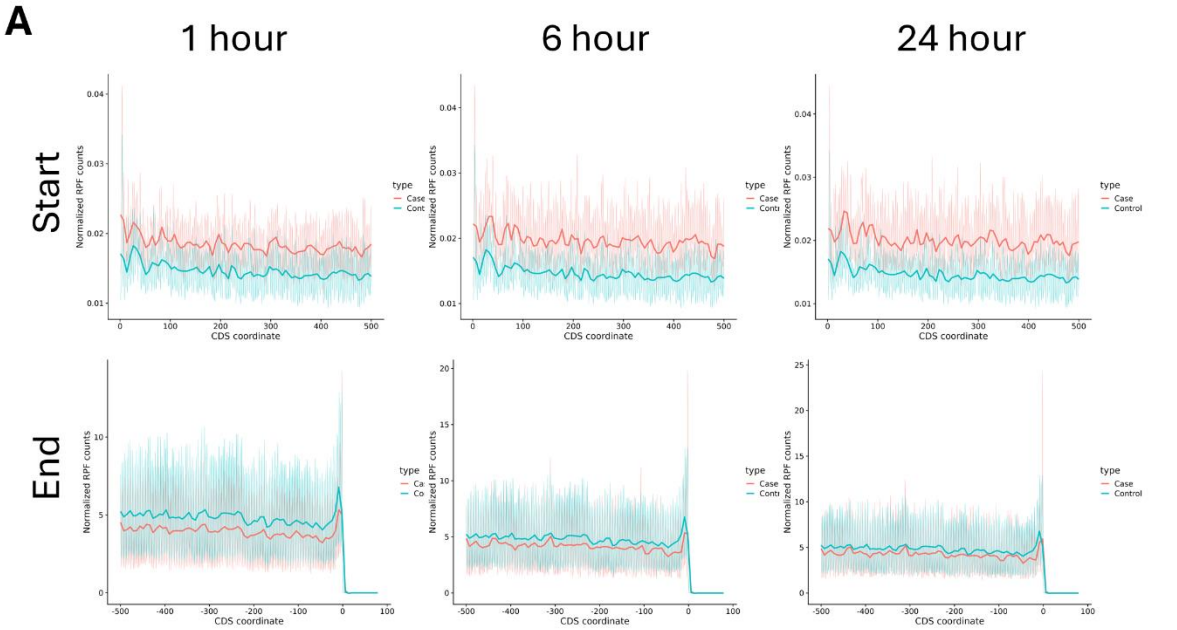

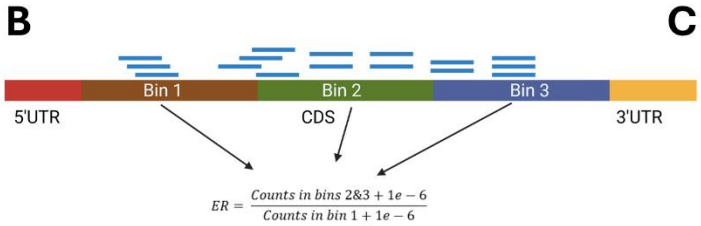

C

	Up	Down
1hr vs Sham	43	40
6hrs vs Sham	585	386
24hrs vs Sham	734	549

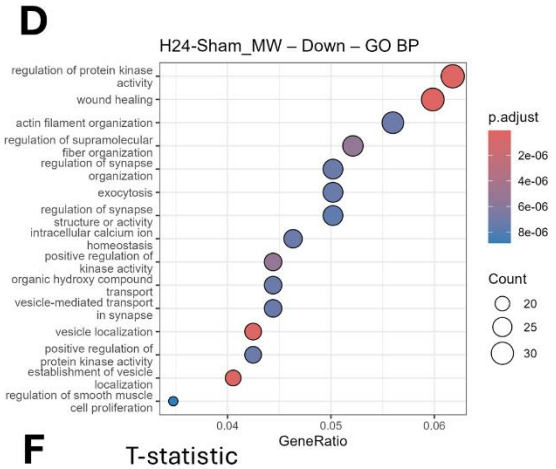

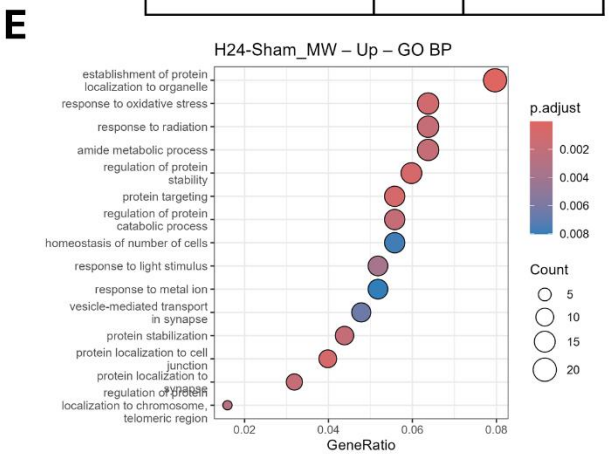

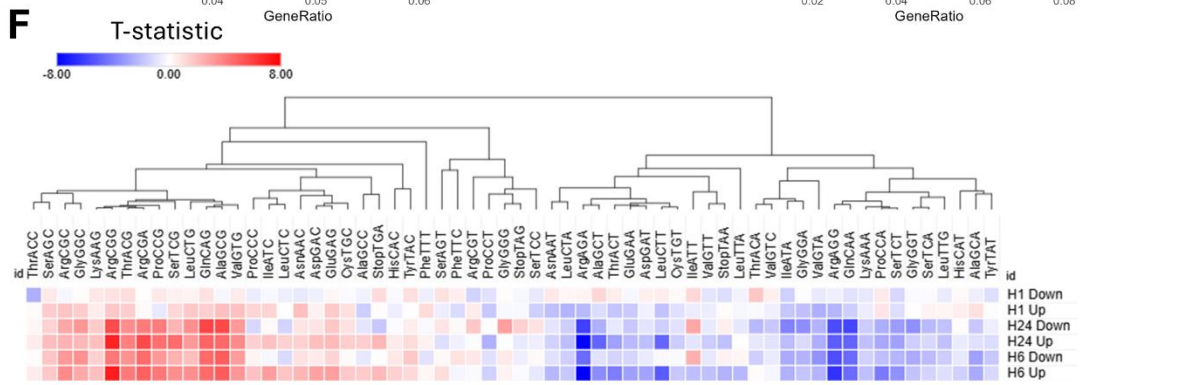

Figure 4: Stroke induces global alterations in the ribosomal reading frame. A-C: Volcano plots of differential frameshifting after stroke compared to Sham. **D:** The number of genes showing statistically significant changes in their reading frame on Mann-Whitney U test. **E:** GC3 analysis of differentially frameshifted genes at 6- and 24-hours after stroke versus Sham. **F-I:** ORA-GOBP analysis of differentially frameshifted genes at 6- and 24-hours after stroke versus Sham.

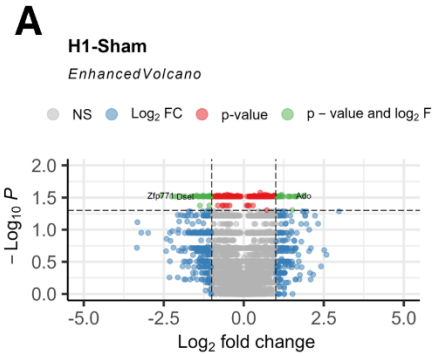

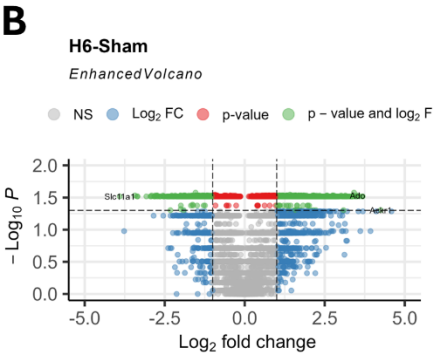

D

Grp vs Sham	Up	Down
1hr	30	38
6hrs	1365	719
24hrs	1613	932

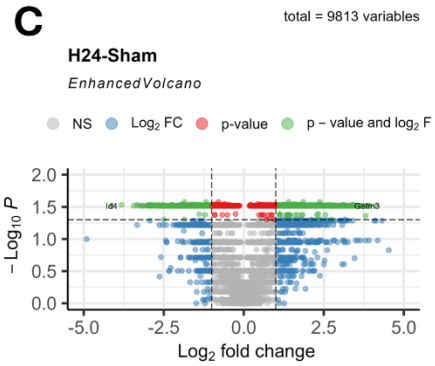

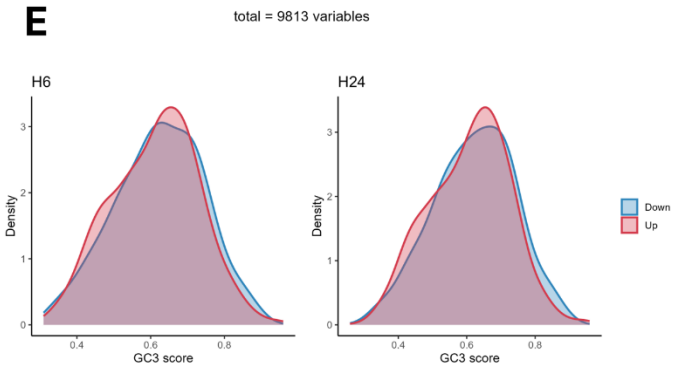

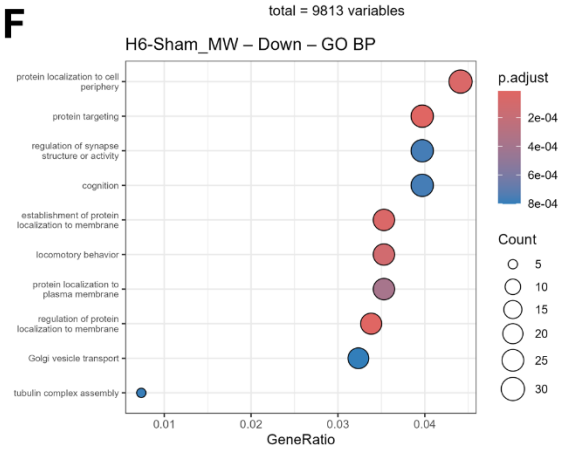

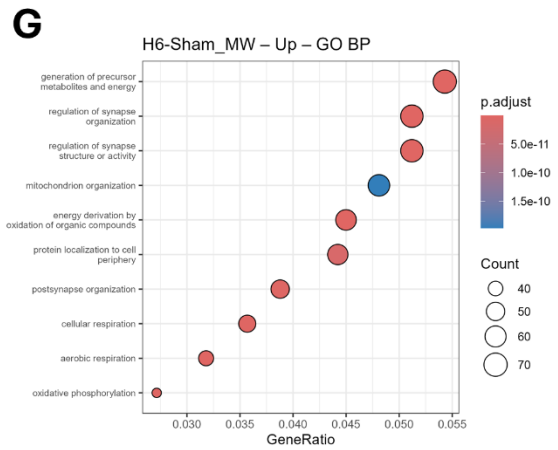

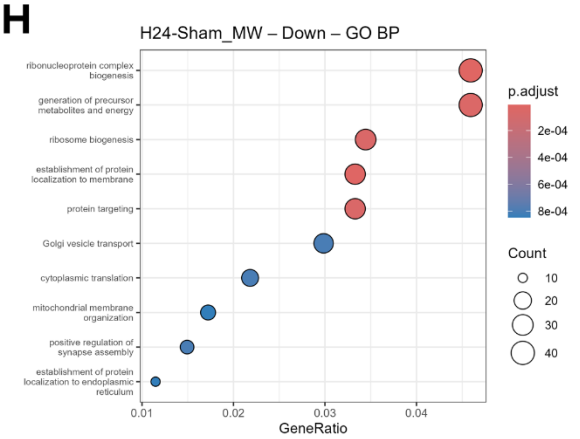

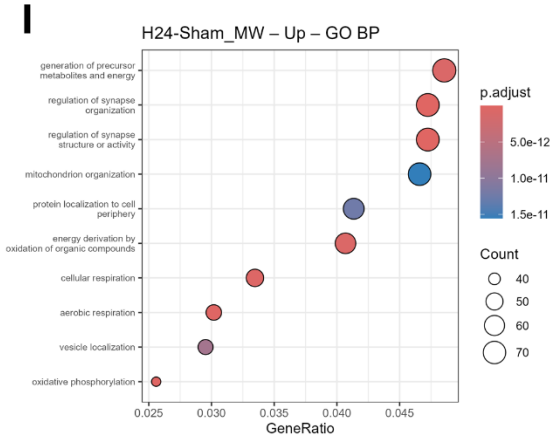

Figure 5: Stroke induces acute transient stop codon readthrough (SCRT). A: Schematic showing the methodology used to calculate the RRS score to identify genes with SCRT events, Higher RRS indicates more SCRT events. When compared to Sham, upregulated genes indicate significant SCRT events in the condition versus Sham and vice versa. **B:** Table showing the number of significant genes with SCRT events in each group versus Sham. **C:** P-site density metagene plots showing the presence of true P-sites in the 3'UTR at the one-hour time point only. Top plot shows a full metagene plot (downstream from start codon and up/downstream from stop codon) of a biological replicate from the 1-hour group. Lower metagene plots showing the up/downstream of the stop codon metagene plots for example samples from each group. True P-sites were only observed in the 1-hour group. **D:** Ercc6 gene metagene plot showing the presence of true ribosome footprint in the 3'UTR in the 1-hour group around 150 nucleotides downstream of the stop codon. **E:** Mrpl10 gene metagene plot showing the presence of true ribosome footprint in the 3'UTR in the 1-hour group around 50~70 nucleotides downstream of the stop codon.

A

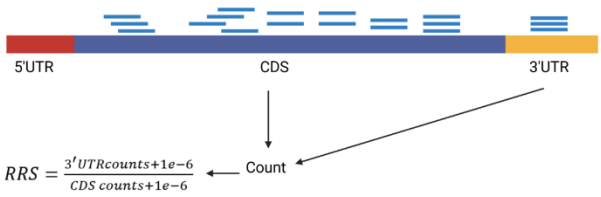

B

Comparison	Up	Down
1hr vs Sham	324	59
6hrs vs Sham	205	408
24hrs vs Sham	261	549

C

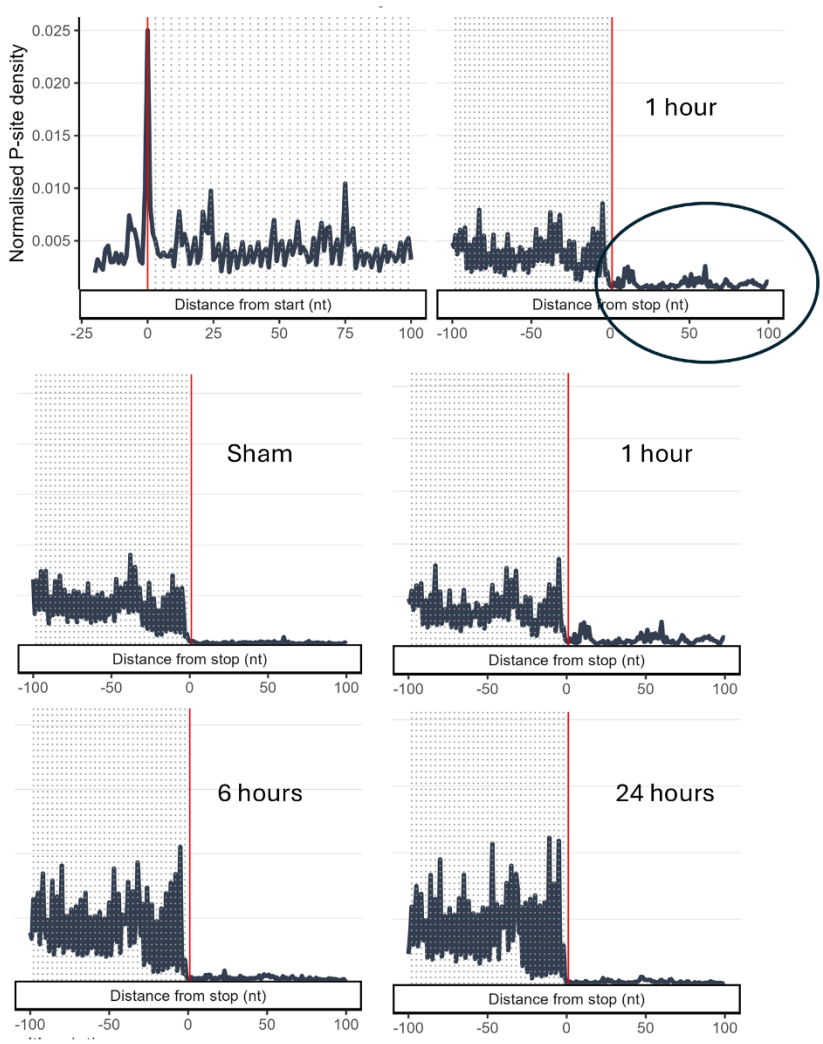

D

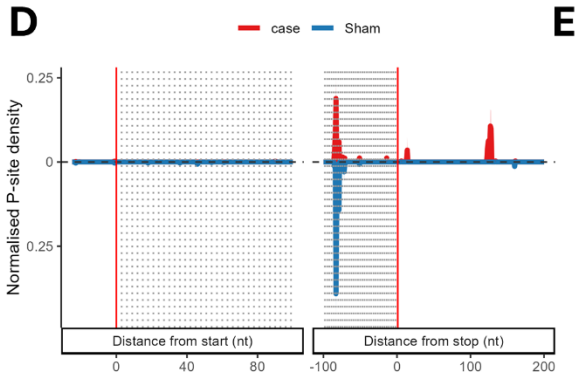

E

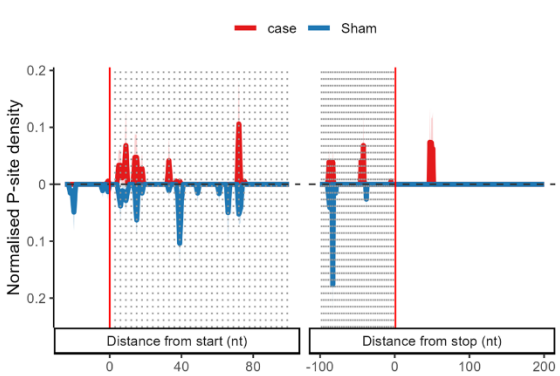

Figure 6: A: ORA-GOBP analysis of the upregulated genes in the SCRT analysis 1-hour after stroke (i.e. those with increased SCRT compared to Sham). **B:** GC3 analysis of the up and downregulated genes in the SCRT analysis of 1-hour group versus Sham. **C:** Isoacceptors codon frequencies analysis of genes with significant SCRT events at the 1-hour timepoint versus Sham. **D:** Analysis of stop codon context. This heatmap indicates the percentage of occurrence of statistically significant codons 5 frames upstream and downstream of the stop codon compared to the background (i.e. entire transcriptome).

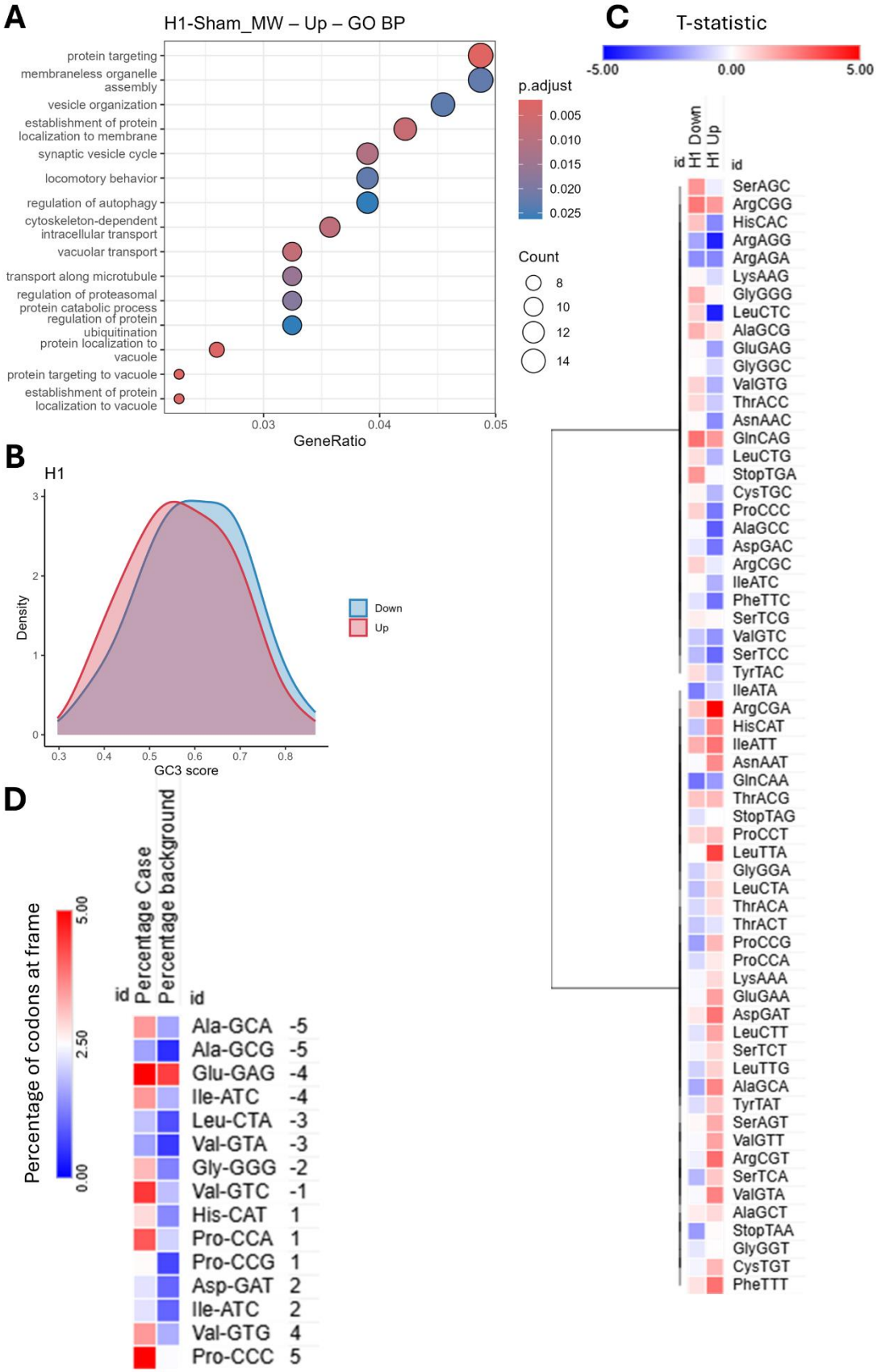
A
H1-Sham_MW – Up – GO BP
protein targeting
membraneless organelle assembly
vesicle organization
establishment of protein localization to membrane
synaptic vesicle cycle
locomotory behavior
regulation of autophagy
cytoskeleton-dependent intracellular transport
vacuolar transport
transport along microtubule
regulation of proteasomal protein catabolic process
regulation of protein ubiquitination
protein localization to vacuole
protein targeting to vacuole
establishment of protein localization to vacuole
0.03
0.04
0.05
GeneRatio
p.adjust
0.005
0.010
0.015
0.020
0.025
Count
8
10
12
14
B
H1
Density
GC3 score
Down
Up
C
T-statistic
-5.00
0.00
5.00
id
H1 Down
H1 Up
SerAGC
ArgCGG
HisCAC
ArgAGG
ArgAGA
LysAAG
GlyGGG
LeuCTC
AlaGCG
GluGAG
GlyGGC
ValGTG
ThrACC
AsnAAC
GlnCAG
LeuCTG
StopTGA
CysTGC
ProCCC
AlaGCC
AspGAC
ArgCGC
IleATC
PheTTC
SerTCG
ValGTC
SerTCC
TyrTAC
IleATA
ArgCGA
HisCAT
IleATT
AsnAAT
GlnCAA
ThrACG
StopTAG
ProCCT
LeuTTA
GlyGGA
LeuCTA
ThrACA
ThrACT
ProCCG
ProCCA
LysAAA
GluGAA
AspGAT
LeuCTT
SerTCT
LeuTTG
AlaGCA
TyrTAT
SerAGT
ValGTT
ArgCGT
SerTCA
ValGTA
AlaGCT
StopTAA
GlyGGT
CysTGT
PheTTT
D
Percentage of codons at frame
5.00
2.50
0.00
id
Percentage Case
Percentage background
Ala-GCA -5
Ala-GCG -5
Glu-GAG -4
Ile-ATC -4
Leu-CTA -3
Val-GTA -3
Gly-GGG -2
Val-GTC -1
His-CAT 1
Pro-CCA 1
Pro-CCG 1
Asp-GAT 2
Ile-ATC 2
Val-GTG 4
Pro-CCC 5

Supplementary figures:

Supplementary figure 1: A: Upset plot showing the shared and unique statistically significant genes in each time-point compared to sham. **B-D:** Spearman's rank correlation analysis using the gene log2 fold change as input comparing between different time points after stroke.

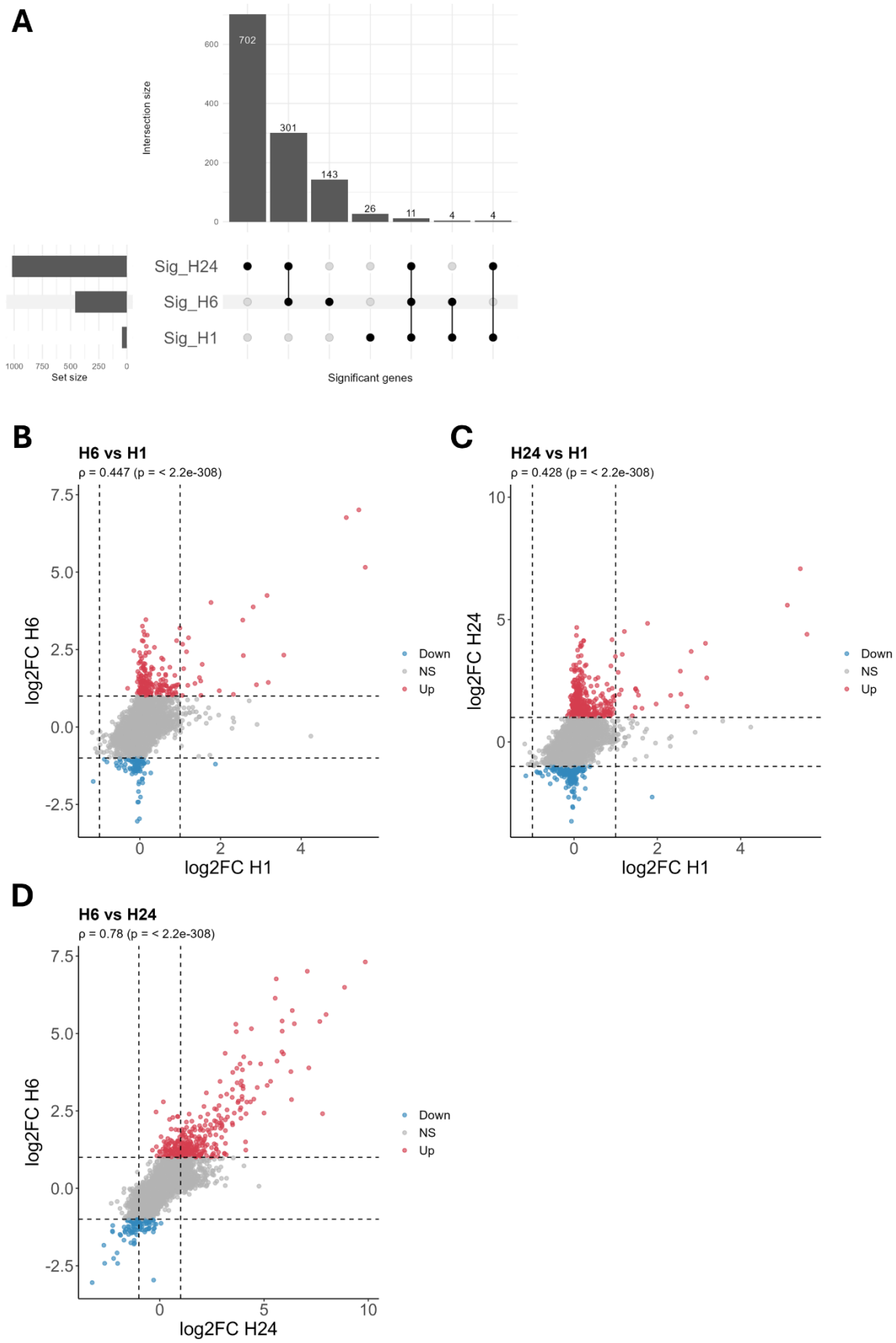
A
Intersection size
702
301
143
26
11
4
4
Sig_H24
Sig_H6
Sig_H1
Set size
Significant genes
B
H6 vs H1
ρ = 0.447 (p = < 2.2e-308)
log2FC H6
log2FC H1
Down
NS
Up
C
H24 vs H1
ρ = 0.428 (p = < 2.2e-308)
log2FC H24
log2FC H1
Down
NS
Up
D
H6 vs H24
ρ = 0.78 (p = < 2.2e-308)
log2FC H6
log2FC H24
Down
NS
Up

Supplementary figure 2: Overrepresentation gene ontology biological processes analysis (ORA-GOBP) of statistically significant genes at each time point.

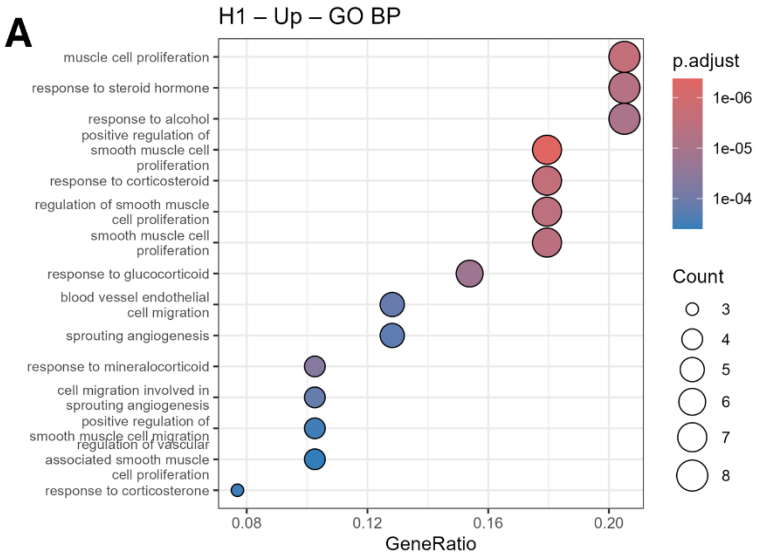
A
H1 – Up – GO BP
muscle cell proliferation
response to steroid hormone
response to alcohol
positive regulation of smooth muscle cell proliferation
response to corticosteroid
regulation of smooth muscle cell proliferation
smooth muscle cell proliferation
response to glucocorticoid
blood vessel endothelial cell migration
sprouting angiogenesis
response to mineralocorticoid
cell migration involved in sprouting angiogenesis
positive regulation of smooth muscle cell migration
regulation of vascular associated smooth muscle cell proliferation
response to corticosterone
0.08
0.12
0.16
0.20
GeneRatio
p.adjust
1e-06
1e-05
1e-04
Count
3
4
5
6
7
8

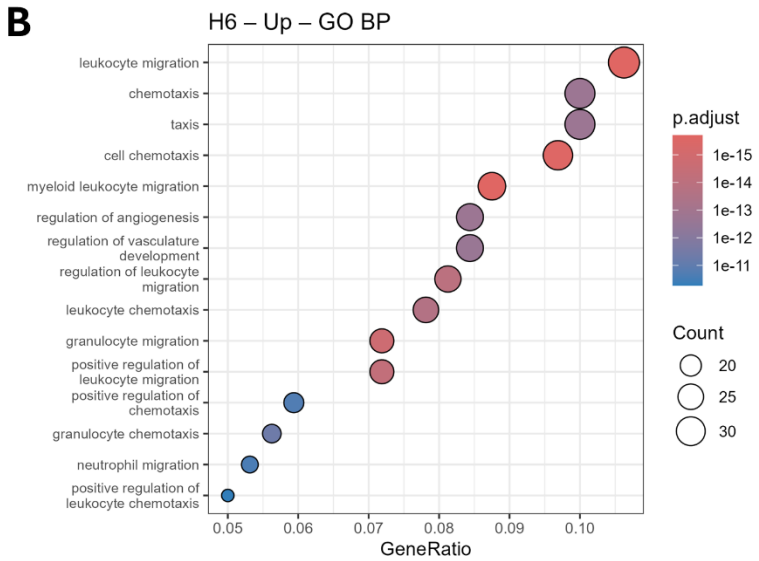
B
H6 – Up – GO BP
leukocyte migration
chemotaxis
taxis
cell chemotaxis
myeloid leukocyte migration
regulation of angiogenesis
regulation of vasculature development
regulation of leukocyte migration
leukocyte chemotaxis
granulocyte migration
positive regulation of leukocyte migration
positive regulation of chemotaxis
granulocyte chemotaxis
neutrophil migration
positive regulation of leukocyte chemotaxis
0.05
0.06
0.07
0.08
0.09
0.10
GeneRatio
p.adjust
1e-15
1e-14
1e-13
1e-12
1e-11
Count
20
25
30

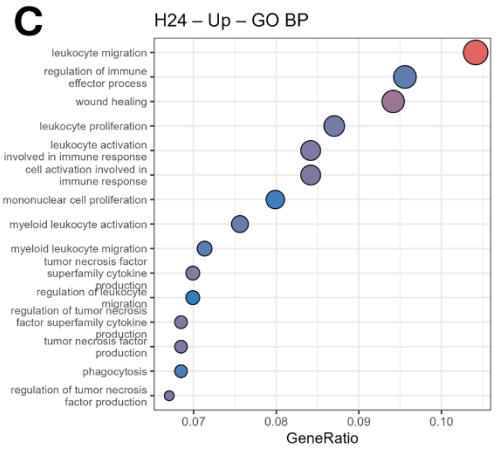
C
H24 – Up – GO BP
leukocyte migration
regulation of immune effector process
wound healing
leukocyte proliferation
leukocyte activation involved in immune response
cell activation involved in immune response
mononuclear cell proliferation
myeloid leukocyte activation
myeloid leukocyte migration
tumor necrosis factor superfamily cytokine production
regulation of leukocyte migration
regulation of tumor necrosis factor superfamily cytokine production
tumor necrosis factor production
phagocytosis
regulation of tumor necrosis factor production
0.07
0.08
0.09
0.10
GeneRatio
p.adjust
1e-35
1e-32
1e-29
Count
50
55
60
65
70

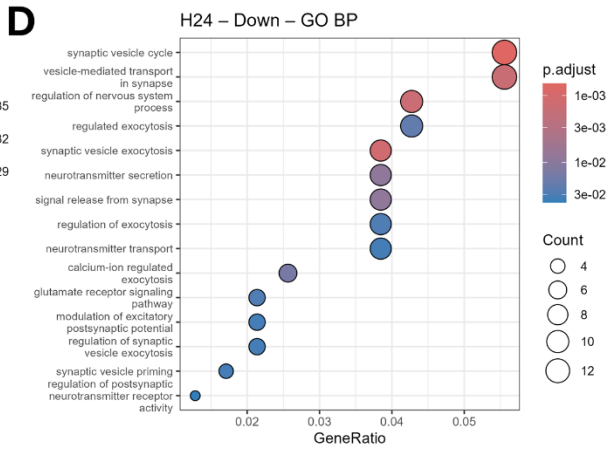
D
H24 – Down – GO BP
synaptic vesicle cycle
vesicle-mediated transport in synapse
regulation of nervous system process
regulated exocytosis
synaptic vesicle exocytosis
neurotransmitter secretion
signal release from synapse
regulation of exocytosis
neurotransmitter transport
calcium-ion regulated exocytosis
glutamate receptor signaling pathway
modulation of excitatory postsynaptic potential
regulation of synaptic vesicle exocytosis
synaptic vesicle priming
regulation of postsynaptic neurotransmitter receptor activity
0.02
0.03
0.04
0.05
GeneRatio
p.adjust
1e-03
3e-03
1e-02
3e-02
Count
4
6
8
10
12

Supplementary figure 3: ORA-GOBP analysis of genes with statistically significant changes in their elongation dynamics in the 1- and 6-hour groups versus Sham.

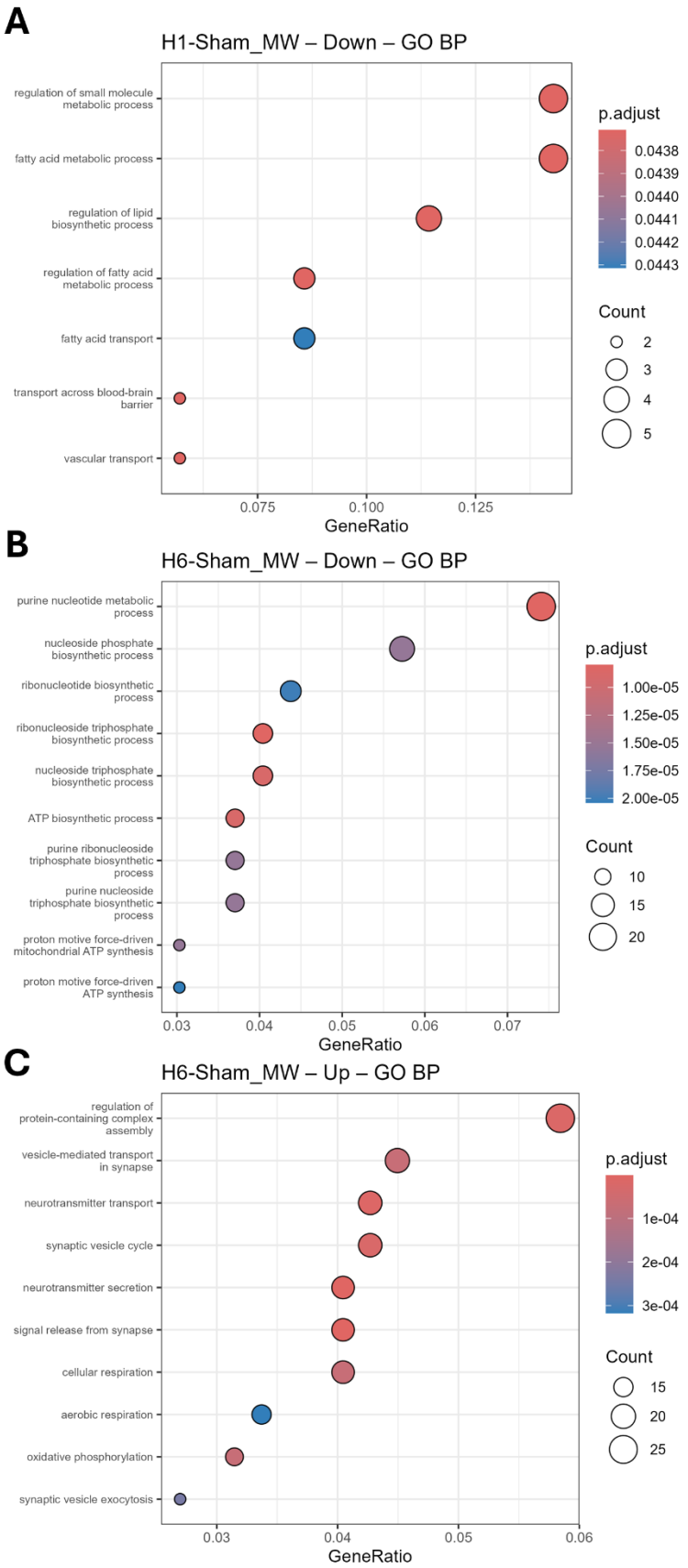
A
H1-Sham_MW – Down – GO BP
regulation of small molecule metabolic process
fatty acid metabolic process
regulation of lipid biosynthetic process
regulation of fatty acid metabolic process
fatty acid transport
transport across blood-brain barrier
vascular transport
0.075
0.100
0.125
GeneRatio
p.adjust
0.0438
0.0439
0.0440
0.0441
0.0442
0.0443
Count
2
3
4
5
B
H6-Sham_MW – Down – GO BP
purine nucleotide metabolic process
nucleoside phosphate biosynthetic process
ribonucleotide biosynthetic process
ribonucleoside triphosphate biosynthetic process
nucleoside triphosphate biosynthetic process
ATP biosynthetic process
purine ribonucleoside triphosphate biosynthetic process
purine nucleoside triphosphate biosynthetic process
proton motive force-driven mitochondrial ATP synthesis
proton motive force-driven ATP synthesis
0.03
0.04
0.05
0.06
0.07
GeneRatio
p.adjust
1.00e-05
1.25e-05
1.50e-05
1.75e-05
2.00e-05
Count
10
15
20
C
H6-Sham_MW – Up – GO BP
regulation of protein-containing complex assembly
vesicle-mediated transport in synapse
neurotransmitter transport
synaptic vesicle cycle
neurotransmitter secretion
signal release from synapse
cellular respiration
aerobic respiration
oxidative phosphorylation
synaptic vesicle exocytosis
0.03
0.04
0.05
0.06
GeneRatio
p.adjust
1e-04
2e-04
3e-04
Count
15
20
25

Supplementary figure 4: Isoacceptors codon frequencies analysis of differentially frameshifted genes after stroke versus Sham.

A

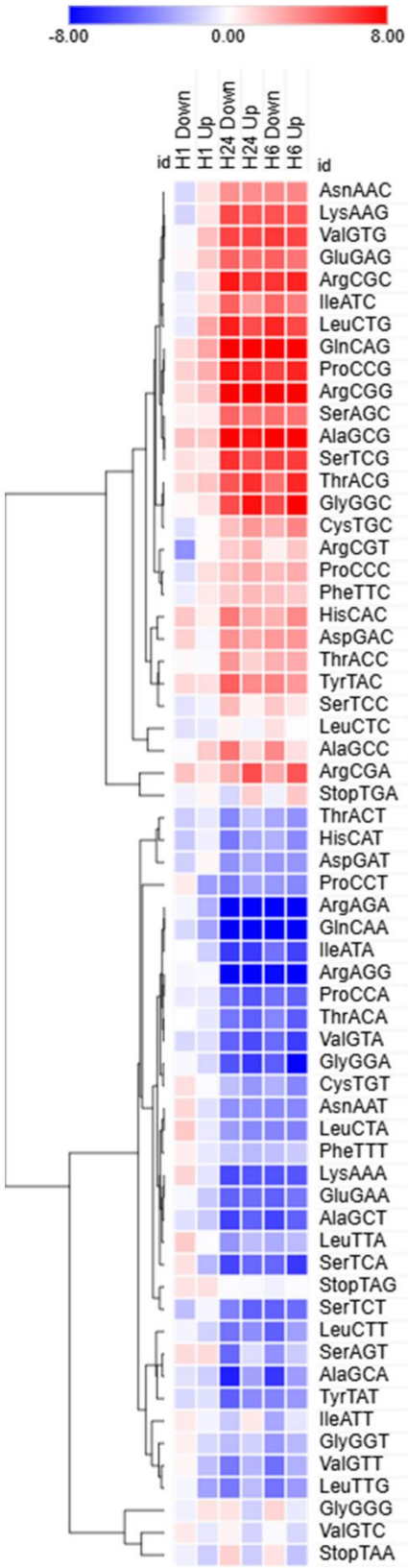
-8.00
0.00
8.00
id
H1 Down
H1 Up
H24 Down
H24 Up
H6 Down
H6 Up
id
AsnAAC
LysAAG
ValGTG
GluGAG
ArgCGC
IleATC
LeuCTG
GlnCAG
ProCCG
ArgCGG
SerAGC
AlaGCG
SerTCG
ThrACG
GlyGGC
CysTGC
ArgCGT
ProCCC
PheTTC
HisCAC
AspGAC
ThrACC
TyrTAC
SerTCC
LeuCTC
AlaGCC
ArgCGA
StopTGA
ThrACT
HisCAT
AspGAT
ProCCT
ArgAGA
GlnCAA
IleATA
ArgAGG
ProCCA
ThrACA
ValGTA
GlyGGA
CysTGT
AsnAAT
LeuCTA
PheTTT
LysAAA
GluGAA
AlaGCT
LeuTTA
SerTCA
StopTAG
SerTCT
LeuCTT
SerAGT
AlaGCA
TyrTAT
IleATT
GlyGGT
ValGTT
LeuTTG
GlyGGG
ValGTC
StopTAA